RSC Advances

PAPER

View Article Online
View Journal | View Issue

Cite this: RSC Adv., 2015, 5, 5958

Visible light driven reduction of carbon dioxide with water on modified $Sr_3Ti_2O_7$ catalysts

Velu Jeyalakshmi,[ac] Rajaram Mahalakshmy,[a] Kanaparthi Ramesh,[b] Peddy V. C. Rao,[b] Nettem V. Choudary,[b] Gandham Sri Ganesh,[b] Kandasamy Thirunavukkarasu,[c] Konda Ramasamy Krishnamurthy[c] and Balasubramanian Viswanathan*[c]

Received 8th October 2014
Accepted 8th December 2014

DOI: 10.1039/c4ra11985a

www.rsc.org/advances

Layered perovskite type $Sr_3Ti_2O_7$ catalysts, doped with N, S and Fe have been prepared by modified polymer complex method, characterized and evaluated for photo reduction of CO_2 in aqueous alkaline medium using UV-visible radiation. EDXA and XRD data reveal the incorporation of the dopants into the titanate matrix. The presence of N in substitutional and interstitial locations, S as S^{6+} and Fe as Fe^{3+} species are indicated by XPS analysis. DRS and photo luminescence studies show that the dopants form additional energy levels within the band gap, promoting visible light absorption and retarding recombination of the charge carriers. Morphological changes and smaller crystallites also minimize recombination. Layered structure of $Sr_3Ti_2O_7$ facilitates easy transport of charge carriers and separation of oxidation/reduction reaction centres. Structural, morphological and photo physical characteristics of doped catalysts improve the activity significantly. $Sr_3Ti_2O_7$ co-doped with N, S and Fe together, displays maximum apparent quantum yield for CO_2 reduction products.

Introduction

The photocatalytic reduction of CO_2 (PCRC) with water to yield hydrocarbons or artificial photo synthesis is a topic for intense investigations due to its scientific as well as technological importance.[1] The process is considered as one of the options for moderation of global warming due to the rising levels of atmospheric CO_2 and the possible use of CO_2 as an alternative source for energy.[2] A wide range of binary/ternary and multi component semi-conducting oxides[3] have been explored for CO_2 photo reduction. The most essential characteristics of a viable catalyst for this application are[4]

(a) The valence band top energy level has to be more positive with respect to the oxidation potential for water.

(b) The conduction band bottom energy level has to be more negative with respect to the reduction potential for CO_2.

TiO_2, ZnO, CdS, GaP, SiC, $SrTiO_3$ are some of the oxides that satisfy the above criteria. While majority of the PCRC studies are concerned with titania and its modified versions[5] as catalysts, several mixed metal oxide semi-conductors like, $NaTaO_3$,[6] $ZnGa_2O_4$[7] and Zn_2GeO_4[8] along with a range of promoters/co-catalysts have been explored for this application. Mixed metal oxides that belong to the family of perovskites, ABO_3, like $SrTiO_3$[9] and $NaTaO_3$[10] with various co-catalysts Pt, Ag, Au, CuO, NiO and RuO_2 display significant and stable activity for photo reduction of CO_2. In addition, perovskites with layered structure like, $ALa_4Ti_4O_{15}$ (A = Ca, Sr, Ba) with Ag as co-catalyst[11] exhibit better performance, since the layered structure facilitates faster transport of charge carriers and the interlayer space could be used as oxidation/reduction reaction sites, leading to the separation of charge carriers.[12]

In this report, we present our results on CO_2 photo reduction on another layered perovskite $Sr_3Ti_2O_7$, which in combination with NiO as co-catalyst, is known to be an efficient catalyst for photo catalytic splitting of water.[13] Though the parent perovskite $SrTiO_3$, has been explored for PCRC,[9] to the best of our knowledge, there are no such reports on $Sr_3Ti_2O_7$. As shown in Fig. 1, the conduction band bottom energy level is suitable for the subsequent reduction of CO_2 after the initial activation to form $CO_2^{-\bullet}$ and hence $Sr_3Ti_2O_7$ is an ideal candidate for investigation, but for the wider band gap. Incorporation of suitable dopants could render $Sr_3Ti_2O_7$ active in the visible region. Increasing the life time of the photo generated charge carriers is another important factor responsible for improving the efficiency of the photo catalytic reduction. In the present work, the effect of doping/co-doping $Sr_3Ti_2O_7$ with N, S and Fe has been explored in order to achieve reduction in the band gap energy and minimize the charge carrier recombination.

[a]Department of Chemistry, Thiagarajar College, Madurai Kamaraj University, Madurai-625021, India

[b]Corporate R&D Centre, Hindustan Petroleum Corporation Ltd, Bangalore-560066, India

[c]National Centre for Catalysis Research (NCCR), Indian Institute of Technology Madras, Chennai-600036, India. E-mail: bvnathan@iitm.ac.in; Fax: +91 44 22574202; Tel: +91 44 22574241

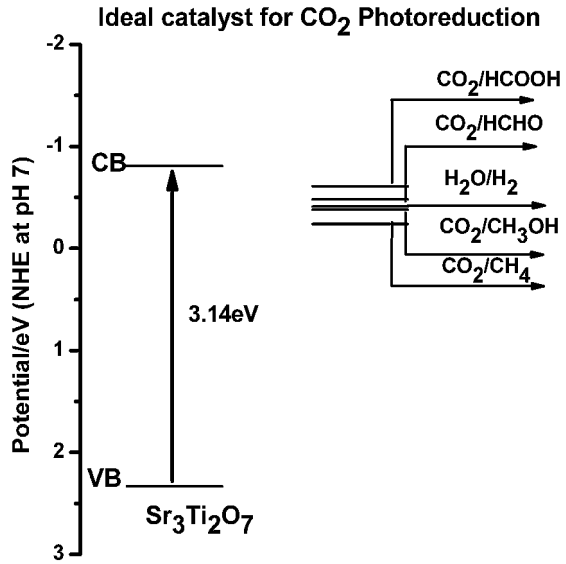

Fig. 1 VB & CB energy levels of $Sr_3Ti_2O_7$ with respect to the potential for reduction of CO_2 and oxidation of water.

Experimental

Preparation of catalysts

Neat $Sr_3Ti_2O_7$ was prepared by adopting polymer complex method, reported by Yoshino *et al.*[14] after some modifications at our end. Ethylene glycol and methanol ratio and pH of the medium were further optimized to get phase pure $Sr_3Ti_2O_7$. Titanium tetra butoxide (2 moles) was added to a mixture of ethylene glycol and methanol (1 : 2 mole ratio) with vigorous stirring. To this mixture, citric acid (to get 1 : 0.5 mole ratio of glycol:citric acid) and strontium nitrate (3 moles as per the stoichiometry) were added. Heating the mixture at 130 °C for 20 h resulted in a polymer complex gel, which was pyrolized in air at 350 °C, followed by calcination at 900 °C for 2 h. Urea or thio-urea (2 moles in each case) as precursors for N doping and NS co-doping and Fe_2O_3 powder (3 wt% with respect to $Sr_3Ti_2O_7$) as such, were introduced along with strontium nitrate, prior to polyester formation to obtain doped $Sr_3Ti_2O_7$. Doped catalysts are represented by the general formulae-$Sr_3Ti_2O_7$ (neat), $Sr_3Ti_2O_{(7-x)}N_x$, $Sr_3Ti_{(2-x)}S_xO_{(7-y)}N_y$, $Sr_3Ti_{(2-x)}Fe_xO_7$, $Sr_3Ti_{(2-x)}Fe_xO_{(7-y)}N_y$, $Sr_3Ti_{(2-x-y)}Fe_xS_yO_{(7-z)}N_z$ signifying different dopant compositions.

Characterization

The crystal phase of the catalysts was analysed by X-ray diffractometer (Rigaku-MiniFlex-II) using Cu Kα radiation (λ = 1.54056 Å) with the scan range of 2θ = 5–90° at a speed of 3° min^{-1}. The crystallite sizes were calculated by the Scherrer's formula, $t = K\lambda/\beta \cos\theta$, where t is the crystallite size, K is the constant dependent on crystallite shape (0.9 for this case) and λ = 1.54056 Å, β is the FWHM (full width at half maximum) and θ is the Bragg's angle.

Diffuse reflectance absorption spectra of the catalysts in the UV-visible region were recorded using a Thermo Scientific Evolution 600 spectrophotometer equipped with a Praying Mantis diffuse reflectance accessory.

Photo luminescence spectra were recorded under excitation with a 450 W xenon lamp and the data were collected using Jobin Yvon Fluorolog 3-11 spectrofluorometer.

Surface area of the catalysts was measured using Micromeritics ASAP 2020. Samples were degassed at 373 K for 2 h and at 423 K for 3 h. Pure nitrogen at liquid nitrogen temperature (77 K) was used as the adsorbate.

Scanning electron micrographs and elemental analysis by EDXA were recorded using FEI, Quanta 200 SEM unit with EDXA attachment. The samples in powder form were taken on the carbon tape and mounted on the SEM sample holder.

The X-ray photoelectron spectra of the catalysts were recorded using Omicron Nanotechnology instrument with Mg K_α radiation. The base pressure of the analysis chamber during the scan was 2×10^{-10} millibar. The pass energies for individual scan and survey scan are 20 and 100 eV, respectively. The spectra were recorded with step width of 0.05 eV. The data were processed with the Casa XPS program (Casa Software Ltd, UK), and calibrated with reference to the adventitious carbon peak (284.9 eV) in the sample. Peak areas were determined by integration employing a Shirley-type background. Peaks were considered to be a 70 : 30 mix of Gaussian and Lorentzian functions. The relative sensitivity factors (RSF) were obtained from literature.

Photo catalytic reduction

Activity of the catalysts in UV visible region (300–700 nm) was evaluated in batch mode using jacketed all glass reactor (620 ml)[15] fitted with quartz window (5 cm dia) and filled with 400 ml of aqueous 0.2 N NaOH solution to increase the solubility of CO_2 and act as hole scavenger. 0.4 g of catalyst was dispersed in the alkaline solution with vigorous stirring (400 rpm). Increasing the stirring rate beyond 400 rpm did not affect the conversion, indicating that under the present experimental conditions, the mass transfer limitations are overcome at this rate. Aqueous alkaline solution (pH-13.0) was saturated with CO_2 by continuous bubbling for 30 minutes after which pH turned 8.0. Reactor in-let and out-let valves were then closed and irradiation with Hg lamp with 77 W power (from WACOM HX-500 lamp house) was started. Gas and liquid phase samples at periodic intervals were taken out with gas-tight/liquid syringes and analysed by GC. Liquid phase products (hydrocarbons) were analysed on PoroPlot Q capillary column with FID and gas phase products on Molecular Sieve 13× column with TCD. Potassium ferric oxalate was used as standard for actinometry. Apparent quantum yield (AQY) was calculated based on the quantities of different products formed per hour and using the formula

$$\mathrm{AQY}(\%) = \frac{\text{number of reacted electrons}}{\text{number of incident photons}} \times 100$$

Blank experiments (reaction with irradiation without catalyst and reaction in dark with catalyst) were conducted to ensure

that the products formed were due to photo reduction of CO_2. When the solution with dispersed catalyst was purged, saturated with nitrogen and irradiated, very small quantities of hydrocarbons, possibly due to the conversion of residual carbon on catalyst surface, was observed up to six hours, after which no product could be detected. However, on purging and saturation with CO_2, hydrocarbons in increasing amounts up to 20 h and beyond could be observed, thus establishing that the products are actually due to PCRC. Based on these observations, with each catalyst composite, the solution saturated with nitrogen was first irradiated for 12 h to remove hydrocarbons formed from carbon residues and then saturated with CO_2 so that PCRC on clean catalyst could be followed further for 20 h.

Results and discussions

Characterization of the catalysts

All the characteristic d-lines for $Sr_3Ti_2O_7$ phase[13] are observed in the XRD patterns for neat and doped samples (Fig. 2).

The amount of dopants being small, no major changes in the XRD patterns for the doped samples are observed, except for a small shift in d-lines for Fe doped samples, as shown in Fig. 3. This shift in d-line could be due to the location of doped Fe^{3+} ions with ionic radius of 0.64 Å in Ti^{4+} ion (0.61 Å) sites.

SE micrograph for the neat $Sr_3Ti_2O_7$ as shown in Fig. 4 reveals a distinct plate like morphology. Doping with N, S and Fe brings out perceptible changes in the morphology. A gradual decrease in crystallite size, as measured by X-ray line broadening analysis of doped $Sr_3Ti_2O_7$ catalysts, is observed (Table 1).

Preparation by polymer complex method has resulted in moderate BET surface area of 25 $m^2\ g^{-1}$ for the neat $Sr_3Ti_2O_7$ sample.

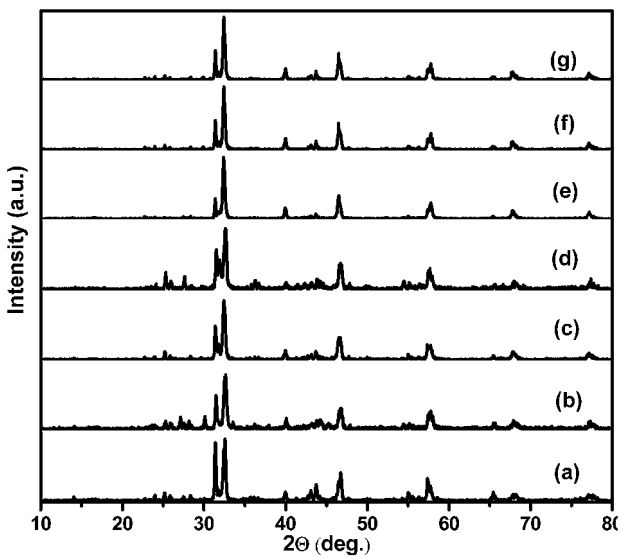

Fig. 2 XRD patterns for neat and doped $Sr_3Ti_2O_7$: (a) $Sr_3Ti_2O_7$, (b) $Sr_3Ti_2O_{(7-x)}N_x$, (c) $Sr_3Ti_{(2-x)}S_xO_{(7-y)}N_y$ (d) $Sr_3Ti_{(2-x)}Fe_xO_7$, (e) $Sr_3Ti_{(2-x)}Fe_xO_{(7-y)}N_y$, (f) $Sr_3Ti_{(2-x-y)}Fe_xS_yO_{(7-z)}N_z$, (g) $Sr_3Ti_{(2-x-y)}Fe_xS_yO_{(7-z)}N_z$-used.

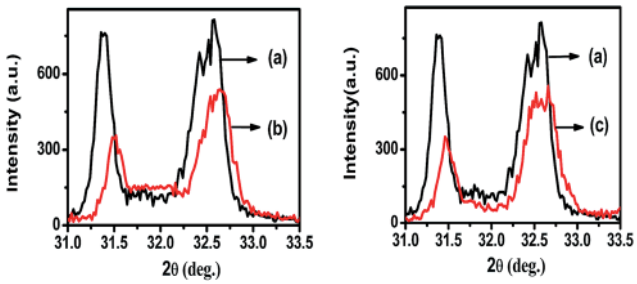

Fig. 3 Shift in d-lines for doped $Sr_3Ti_2O_7$ for (a) $Sr_3Ti_2O_7$, (b) $Sr_3Ti_{(2-x)}Fe_xO_7$, (c) $Sr_3Ti_{(2-x-y)}Fe_xS_yO_{(7-z)}N_z$.

Addition of the dopants prior to polyester/gel formation has ensured effective incorporation of the dopant elements N, S and Fe into the titanate matrix. This aspect is confirmed by the qualitative EDXA spectral data presented in Fig. 5. DRS profiles for neat and doped/co-doped (separately with N, N–S, Fe–N, Fe–N–S and Fe) $Sr_3Ti_2O_7$ catalysts are shown in Fig. 6. Band gap energy of 3.14 eV observed for neat $Sr_3Ti_2O_7$ in the present case is close to the value of 3.2 eV reported earlier.[13]

When doped with N or co-doped with N and S (profiles (b) & (c) in Fig. 6) a distinct shift in light absorption edge, tending towards visible region, is evident. With Fe, either alone or by co-doping with N or N–S, the adsorption edge turns into a near continuum, extending deeper into the visible region and indicating excitations from two different energy levels within the band gap. Reduced band gap energy values, observed for the doped/co-doped catalysts are given in Table 1.

Photo luminescence spectra of the catalysts (Fig. 7) bring out additional features of doped catalysts.

Undoped $Sr_3Ti_2O_7$ shows two photo luminescence (PL) emission lines at 470 nm and 482 nm with significant intensity, arising due to the recombination of charge carriers. With N doping and co-doping of N and S, the intensity of the PL lines is reduced to some extent. However, on doping with Fe

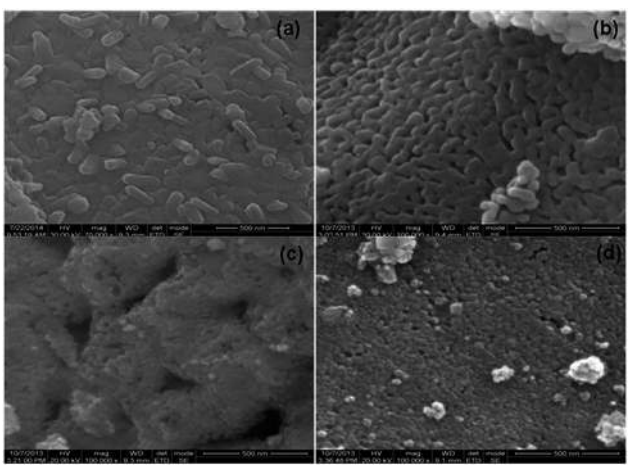

Fig. 4 Changes in the morphology of doped $Sr_3Ti_2O_7$ catalysts-SE micrographs. (a) $Sr_3Ti_2O_7$, (b) $Sr_3Ti_2O_{(7-x)}N_x$, (c) $Sr_3Ti_{(2-x)}S_xO_{(7-y)}N_y$, (d) $Sr_3Ti_{(2-x-y)}Fe_xS_yO_{(7-z)}N_z$.

Table 1 Crystallite size and band gap values for neat and doped $Sr_3Ti_2O_7$ catalysts

Photo catalysts	Crystalline size (nm)	Band gap (eV)
$Sr_3Ti_2O_7$	46.3	3.14
$Sr_3Ti_2O_{(7-x)}N_x$	37.2	2.99
$Sr_3Ti_{(2-x)}S_xO_{(7-y)}N_y$	34.3	2.85
$Sr_3Ti_{(2-x)}Fe_xO_7$	33.5	2.73
$Sr_3Ti_{(2-x)}Fe_xO_{(7-y)}N_y$	24.9	2.57
$Sr_3Ti_{(2-x-y)}Fe_xS_yO_{(7-z)}N_z$	21.9	2.39

and co-doping of Fe with N and N–S, sharp reduction in intensity of the PL lines is observed. Decrease in the intensity of PL lines indicates that the recombination of charge carriers is retarded in presence of the dopants. Such an effect would lead to an increase in the life time of the photo generated electrons and holes and hence, an increase in PCRC activity. These modifications brought out by the dopants in the electronic structure of $Sr_3Ti_2O_7$ have profound influence on the PCRC activity.

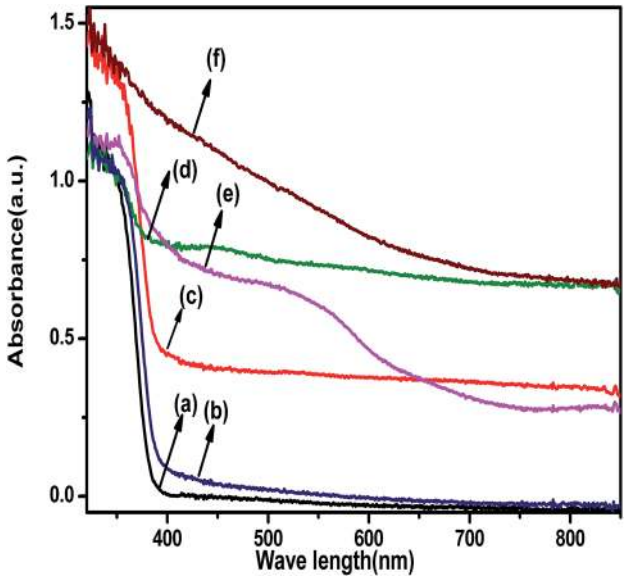

Fig. 6 Diffuse Reflectance spectra for neat and doped $Sr_3Ti_2O_7$ catalysts. (a) $Sr_3Ti_2O_7$, (b) $Sr_3Ti_2O_{(7-x)}N_x$, (c) $Sr_3Ti_{(2-x)}S_xO_{(7-y)}N_y$, (d) $Sr_3Ti_{(2-x)}Fe_xO_7$, (e) $Sr_3Ti_{(2-x)}Fe_xO_{(7-y)}N_y$, (f) $Sr_3Ti_{(2-x-y)}Fe_xS_yO_{(7-z)}N_z$.

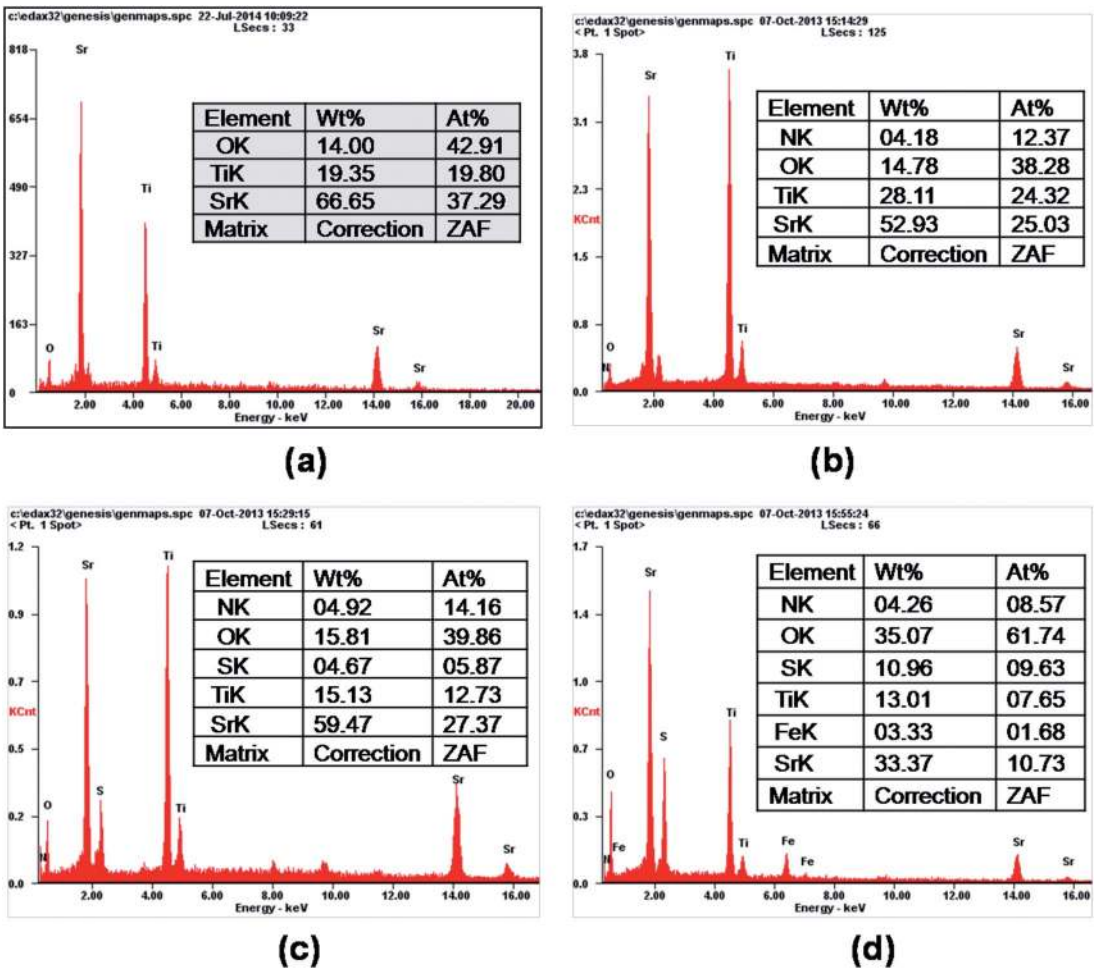

Fig. 5 EDAX spectra and data for neat and doped $Sr_3Ti_2O_7$ catalysts. (a) $Sr_3Ti_2O_7$, (b) $Sr_3Ti_2O_{(7-x)}N_x$, (c) $Sr_3Ti_{(2-x)}S_xO_{(7-y)}N_y$, (d) $Sr_3Ti_{(2-x-y)}Fe_xS_yO_{(7-z)}N_z$.

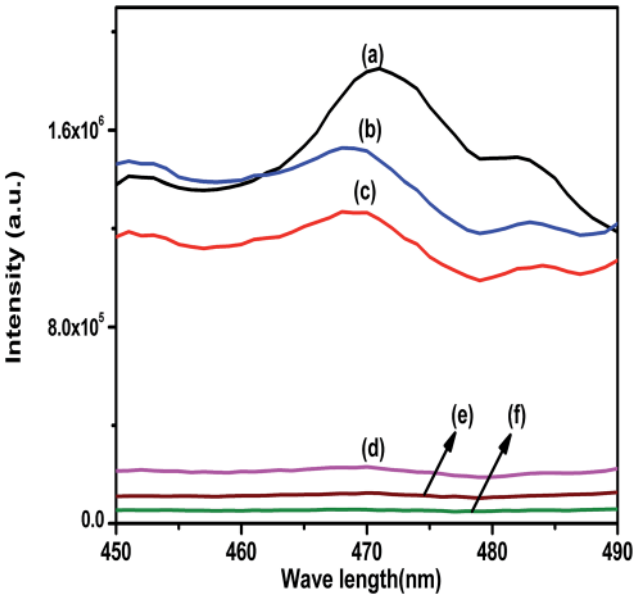

Fig. 7 Photo luminescence spectra for neat and doped $Sr_3Ti_2O_7$ catalysts. (a) $Sr_3Ti_2O_7$, (b) $Sr_3Ti_2O_{(7-x)}N_x$, (c) $Sr_3Ti_{(2-x)}S_xO_{(7-y)}N_y$, (d) $Sr_3Ti_{(2-x)}Fe_xO_{(7-y)}N_y$, (e) $Sr_3Ti_{(2-x-y)}Fe_xS_yO_{(7-z)}N_z$, (f) $Sr_3Ti_{(2-x)}Fe_xO_7$.

Chemical states of the dopants have been analysed by XPS technique (Fig. 8 and 9 and table therein). N1s core level for N doped sample is observed at 398.4 eV. N and S co-doped sample presents a broad profile, which could be resolved into a main peak at 398.5 eV and another of low intensity at 400.6 eV. For Fe, N and S co-doped sample N1s core level is observed at 400.1 eV. N and S co-doped and Fe, N and S co-doped samples show $S2p_{1/2}$ lines at 168.9 and 168.4 eV respectively, due to S^{6+} species. $Fe2p_{3/2}$ lines at 709.4 & 714.0 eV (Fig. 9), are attributed to Fe^{3+} species.

Photo catalytic reduction of CO_2 on neat and doped $Sr_3Ti_2O_7$

Typical trends in product distribution on the neat $Sr_3Ti_2O_7$ and Fe, N and S co-doped $Sr_3Ti_2O_7$, for photo reduction during 20 h on stream period are presented in Fig. 10a and b, these experiments were carried out up to 20 hours. Similar trends are observed on other doped catalysts as well, with variations in the rate and the quantities of products formed. Methanol is the major product, followed by ethanol and acetaldehyde. Methane, ethane and ethylene are formed in trace quantities. Hydrogen and oxygen were also detected in the gas phase. All the catalysts exhibit activity up to 20 h. Rates of formation of products are high during initial 6–8 h beyond which the rate of product formation tends to slow down. Based on the initial rates (upto 10 hours in micro moles g^{-1} h^{-1}) for the formation of different products, and the number of photo electrons involved in each case, apparent quantum yields (AQY) for all the catalysts have been calculated and presented in Table 2 and Fig. 11.

It is clear that doping/co-doping of $Sr_3Ti_2O_7$ with Fe, N and S has brought out significant improvements in the photo catalytic

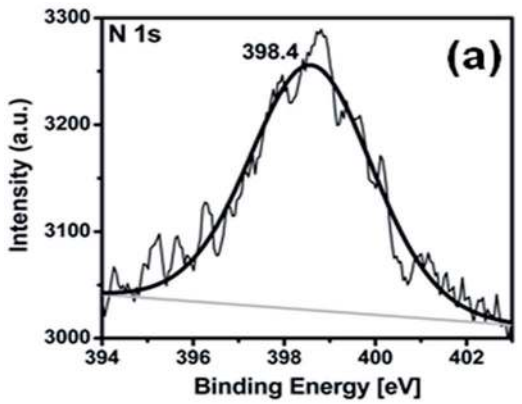

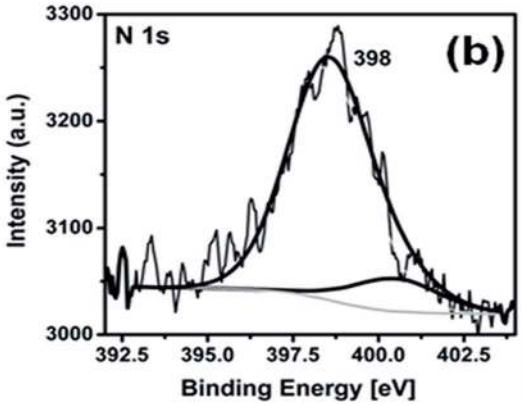

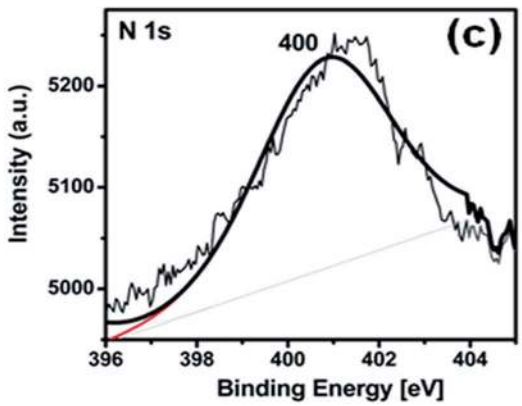

Photocatalyst	Binding Energy (eV)		
	N 1s	S 2p	Fe 2p
$Sr_3Ti_2O_{(7-x)}N_x$	398.4	-	-
$Sr_3Ti_{(2-x)}S_xO_{(7-y)}N_y$	398.5 400.6	168.9	-
$Sr_3Ti_{(2-x-y)}Fe_xS_yO_{(7-z)}N_z$	400.1	168.4	710.4 714.1

Fig. 8 XPS profiles for N1s core level for doped $Sr_3Ti_2O_7$ catalysts (a) $Sr_3Ti_2O_{(7-x)}N_x$, (b) $Sr_3Ti_{(2-x)}S_xO_{(7-y)}N_y$, (c) $Sr_3Ti_{(2-x-y)}Fe_xS_yO_{(7-z)}N_z$.

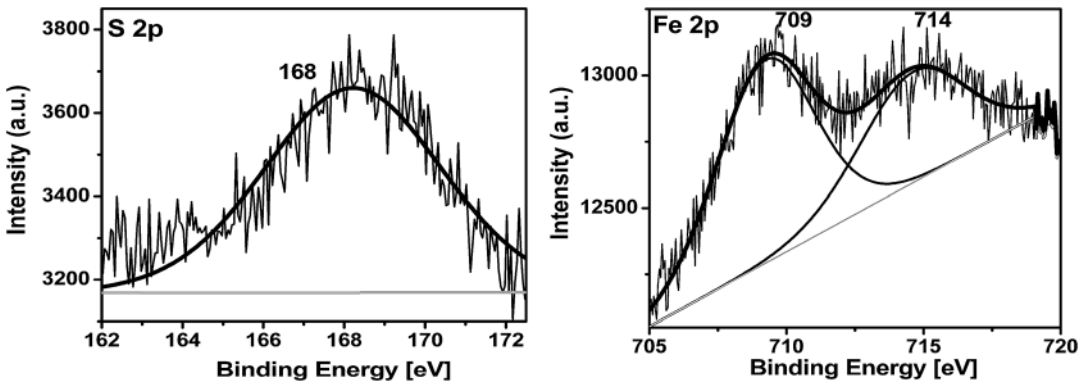

Fig. 9 XPS profiles for S2p & Fe2p levels for $Sr_3Ti_{(2-x-y)}Fe_xS_yO_{(7-z)}N_z$ catalyst.

reduction of CO_2, as indicated by the increase in AQY values. XRD patterns for the fresh Fe, N and S doped $Sr_3Ti_2O_7$ (Fig. 2f) and for the same catalyst after 20 h of use (Fig. 2g), do not reveal any significant changes, indicating structural stability of the catalyst.

Discussions-photo physical characteristics and activity

While the effect of doping $SrTiO_3$ (with cubic perovskite structure) with anions like, N, S and metal oxides (of Fe, Co, Ni and Mn) has been studied in detail,[16–19] to the best of our knowledge, similar investigations on doped $Sr_3Ti_2O_7$ phases have not been reported so far. Structurally, $Sr_3Ti_2O_7$ is closely related to $SrTiO_3$ and is one of the intergrowth phases (known as Ruddlesden Popper-RP phases) formed from $SrTiO_3$ with a general formula SrO $(SrTiO_3)_n$ with $n = 2$. The structural models of the possible RP phases[20] are given in Fig. 12. In $Sr_3Ti_2O_7$ every two cubic perovskite ($SrTiO_3$) layer is separated by a single SrO layer.

The band gap energy values for both $SrTiO_3$ and $Sr_3Ti_2O_7$ are nearly the same (~3.2 eV). While doping $Sr_3Ti_2O_7$ with N reduces the band gap from 3.14 to 2.99 eV (Table 1), co-doping with N and S leads to further reduction to 2.85 eV. This is due to the synergistic effect of co-doping, wherein, the 2p-states of both N and S overlap with that of O2p, leading to narrowing of the band gap. Such effects due to co-doping of N and S have been observed in $SrTiO_3$ and TiO_2.[17,21,22]

N1s core level binding energy value of 398.4 eV observed for N doped $Sr_3Ti_2O_7$, which is close to the value of 398.5 eV reported[23] for nitrogen doped $SrTiO_3$, indicating the presence of anionic nitrogen in substitutional locations of oxygen. Co-doping with N and S shows a main peak at 398.5 eV besides a small intensity peak at 400.6 eV, while with Fe, N and S co-doping, a broad major peak at 400.1 eV is observed, due to nitrogen species in the interstitial locations involving N in different environments like, N–O–Ti–O or O–N–Ti–O.[24,25] These observations are in line with the literature reports[26–28] on nitrogen doping in TiO_2, wherein two energy levels corresponding to substitutional and interstitial nitrogen within the band gap is proposed.

$S2p_{1/2}$ lines observed for N, S and Fe, NS doped $Sr_3Ti_2O_7$ samples at 168.9 and 168.4 eV (table in Fig. 8) respectively shows that S is present as S^{6+} species in the lattice. Presence of

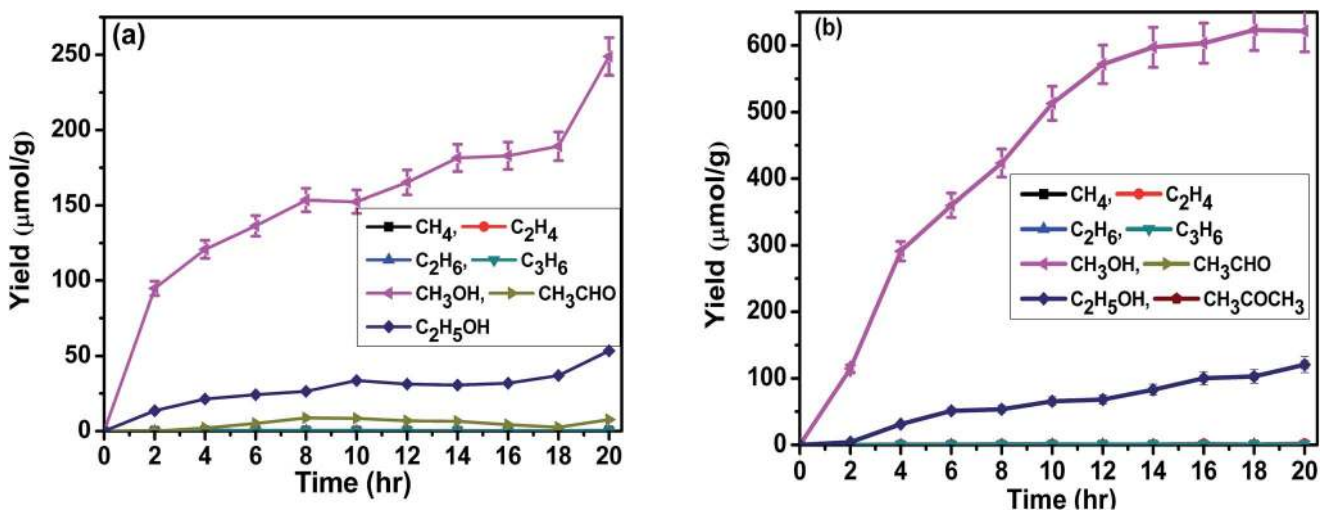

Fig. 10 Trends in products distribution during CO_2 photo reduction (a) $Sr_3Ti_2O_7$ and (b) $Sr_3Ti_{(2-x-y)}Fe_xS_yO_{(7-z)}N_z$ catalysts.

Table 2 Products distribution and quantum yield data for neat and doped $Sr_3Ti_2O_7$ catalysts

	Products obtained from CO_2 reduction ($\mu mol\ g^{-1}\ h^{-1}$)									
Photo catalysts	CH_4	C_2H_4	C_2H_6	CH_3OH	C_2H_4O	C_2H_5OH	C_3H_6O	C_3H_6	H_2	AQY (%)
$Sr_3Ti_2O_7$	0.16	0.08	0.03	19.9	1.5	1.9	—	0.04	1.7	0.003
$Sr_3Ti_2O_{(7-x)}N_x$	0.07	0.01	0.02	21.2	3.1	2.1	—	0.08	1.0	0.005
$Sr_3Ti_{(2-x)}S_xO_{(7-y)}N_y$	0.01	0.04	0.14	41.3	0.1	3.4	0.8	0.01	0.6	0.006
$Sr_3Ti_{(2-x)}Fe_xO_7$	0.23	0.55	0.12	29.9	0.7	6.1	2.7	0.01	0.3	0.006
$Sr_3Ti_{(2-x)}Fe_xO_{(7-y)}N_y$	0.22	0.23	0.19	48.9	0.35	7.8	3.1	0.08	0.5	0.009
$Sr_3Ti_{(2-x-y)}Fe_xS_yO_{(7-z)}N_z$	0.13	1.1	0.3	60.1	3.99	9.9	3.5	0.04	0.7	0.011

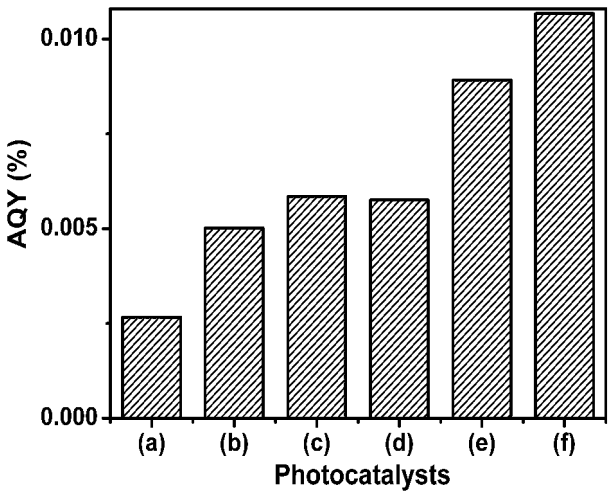

Fig. 11 Apparent quantum yields for CO_2 photo reduction on neat and doped $Sr_3Ti_2O_7$ catalysts. (a) $Sr_3Ti_2O_7$, (b) $Sr_3Ti_2O_{(7-x)}N_x$, (c) $Sr_3Ti_{(2-x)}S_xO_{(7-y)}N_y$, (d) $Sr_3Ti_{(2-x)}Fe_xO_7$, (e) $Sr_3Ti_{(2-x)}Fe_xO_{(7-y)}N_y$, (f) $Sr_3Ti_{(2-x-y)}Fe_xS_yO_{(7-z)}N_z$.

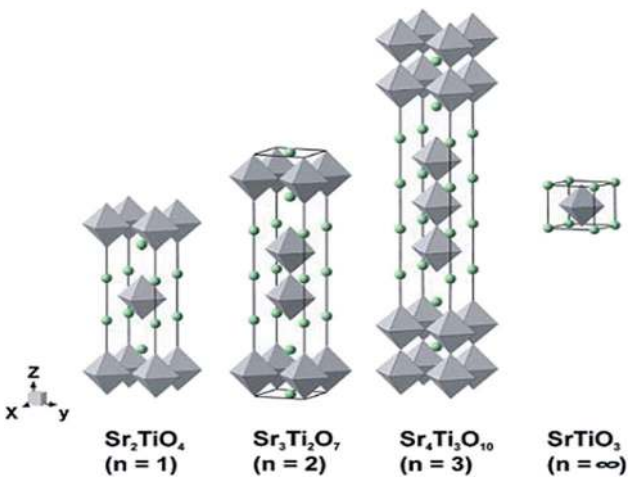

Fig. 12 Structural models of Ruddlesden Popper phases.[20]

S^{2-} species is ruled out, as its ionic size is too large (0.184 nm) to be located in the place of O^{2-} (0.14 nm).

Studies on the effect of doping of $SrTiO_3$ with Fe[21,22] have revealed that additional energy levels identified with Fe^{3+} and Fe^{2+} states are created within the band gap. Excitation of electrons from these levels to the conduction band of $SrTiO_3$ corresponds to light absorption in the visible region. Recently, Zhou *et al.*,[18] based on DFT calculations on the electronic level characteristics Fe doped $SrTiO_3$, have shown that Fe^{3+} ions could take up substitutional sites of Ti^{4+} ions and some Fe 3d states are located just above the top of the O2p valence band. Such a configuration results in narrowing of the band gap. Similar changes occurring in Fe doped $Sr_3Ti_2O_7$ could explain the reduction in band gap values. Shift in the XRD d-lines observed for Fe, N and S co-doped $Sr_3Ti_2O_7$ is indicative of the location of doped Fe^{3+} ions in the titania matrix (Fig. 3). Incorporation of Fe^{3+} in $Sr_3Ti_2O_7$[29] and TiO_2[30] lattice networks have been reported earlier.

Apart from enabling the visible light absorption, Fe doping plays a prominent role amongst the dopants, in increasing the life time of charge carriers. Amongst several metal ions explored as electron traps for titania, Fe^{3+} is considered to be the most effective one[31] as it can easily transform from stable $Fe^{3+}(d^5)$ configuration to relatively unstable $Fe^{2+}(d^6)$, which can again transfer electron to form Fe^{3+}. In this manner, Fe could effectively trap electrons and release it to enable charge migration and interfacial charge transfer. This aspect is very well reflected in the photoluminescence spectra of Fe doped samples (Fig. 7). All the elementary steps in a typical photo chemical reaction like, charge pair generation, charge trapping, charge release and migration and interfacial charge transfer[32,33] could be facilitated by doping with Fe.

As suggested by Cong *et al.* for TiO_2,[34] N doping could help in quenching photo luminescence by trapping of electrons in oxygen vacancies and holes by the doped anionic nitrogen species in the following steps:

$$O_V^0 + e_{CB}^- \rightarrow O_V \quad (1)$$

$$N^- + h_{VB}^+ \rightarrow N^0 \quad (2)$$

It is reported that sulfation of titania surface increases the number and strength of the acid sites, which in turn, retard recombination of charge carriers.[35,36] Such an effect due to sulfur doping would be applicable to sulfated $Sr_3Ti_2O_7$ as well, resulting in the minimization of recombination. All the three dopants play a dual role, of reducing the band gap and minimizing the recombination of charge carriers.

The extension of light absorption edge into visible region and increased life time of charge carriers are the two major factors responsible for the observed increase in PCRC activity (Table 2). Besides, decrease in the crystallite size observed for doped samples, is the other contributing factor, since smaller size could shorten the path length for the diffusion of charge carriers from the bulk to the surface and hence reduce the probability for recombination.[37] Additionally, the layered structure of $Sr_3Ti_2O_7$ facilitates easy transport of charge carriers and separation of oxidation/reduction reaction centres within the interlayer space.[12] The formulation, with co-doping of N, S and Fe together, wherein the influence of these factors is maximum, displays maximum activity (Table 2). Apparent quantum yield for CO_2 conversion on titania P-25, when doped with N and S, under identical experimental conditions, is less, at 0.003% compared to 0.006% for N and S doped $Sr_3Ti_2O_7$. When modified suitably, $Sr_3Ti_2O_7$ could be a better alternative for PCRC application.

Conclusions

Neat and doped $Sr_3Ti_2O_7$ samples have been prepared by modified polymer complex method. The influence of doping has been investigated by detailed characterization of the catalysts with XRD, EDXA, SEM, DRS, photo luminescence and X-ray photo electron spectroscopic techniques. Doping/co-doping with anions N, S and metals like Fe, results in the creation of additional energy levels within the band gap, leading to the absorption of visible light and also minimization of the recombination of charge carriers. Formation of smaller crystallites also reduces the probability for recombination. Layered structure of $Sr_3Ti_2O_7$ facilitates easy transport of charge carriers and separation of oxidation/reduction reaction centers. These factors contribute towards the significant improvement in activity for CO_2 photo reduction on $Sr_3Ti_2O_7$ co-doped with N, S and Fe together, wherein the influence of dopants is maximum.

Acknowledgements

NCCR gratefully acknowledges the continuous and generous support provided to the project, by M/s Hindustan Petroleum Corpn Ltd, Mumbai, the support rendered by the Department of Science & Technology, Govt. of India, New Delhi, for establishing NCCR with all laboratory facilities and Indian Institute of Technology Madras, Chennai, for all administrative and infrastructure support.

Notes and references

1 Y. Izumi, *Coord. Chem. Rev.*, 2013, **257**, 171; V. Jeyalakshmi, K. Rajalakshmi, R. Mahalakshmy, K. R. Krishnamurthy and B. Viswanathan, *Res. Chem. Intermed.*, 2013, **39**, 2565; V. Jeyalakshmi, R. Mahalakshmy, K. R. Krishnamurthy and B. Viswanathan, *Matl. Sci. Form*, Trans Tech. Pub, Switzerland, 2013, 734, pp. 1–62; T. J. Meyer, J. M. Papanikolas and C. M. Heyer, *Catal. Lett.*, 2011, **141**, 1.
2 S. C. Roy, O. K. Varghese, M. Paulose and C. A. Grimes, *ACS Nano*, 2010, **4**, 1259; Z. Jiang, T. Xiao, V. L. Kuznetsov and P. P. Edwards, *Philos. Trans. R. Soc., A*, 2010, **368**, 3343; J. C. S. Wu, *Catal. Surv. Asia*, 2009, **13**, 30; M. A. Scibioh and B. Viswanathan, *Proc. Indian Natl. Sci. Acad., Part A*, 2004, **70**, 407.
3 M. Halmann, *Nature*, 1978, **275**, 115; B. A. Blajeni, M. Halmann and J. Manassen, *Sol. Energy*, 1980, **25**, 165; M. Halmann, M. Ulman and B. A. Blajeni, *Sol. Energy*, 1983, **31**, 429; V. Jeyalakshmi, R. Mahalakshmy, K. R. Krishnamurthy and B. Viswanathan, *Indian J. Chem., Sect. A: Inorg., Bio-inorg., Phys., Theor. Anal. Chem.*, 2012, **51**, 1263; K. Li, D. Martin and J. Tang, *Chin. J. Catal.*, 2011, **32**, 879.
4 T. Inoue, A. Fujishima, S. Konishi and K. Honda, *Nature*, 1979, **277**, 637.
5 V. P. Indrakanti, J. D. Kubicki and H. H. Schobert, *Energy Environ. Sci.*, 2009, **2**, 745; K. Mori, H. Yamashita and M. Anpo, *RSC Adv.*, 2012, **2**, 3165.
6 K. Teramura, H. S.-I. Okuoka, H. Tsuneoka, T. Shishido and T. Tanaka, *Appl. Catal., B*, 2010, **96**, 565.
7 S. C. Yan, S. X. Ouyang, J. Gao, M. Yang, J. Y. Feng, X. X. Fan, L. J. Wan, Z. S. Li, J. H. Ye, Y. Zhou and Z. G. Zou, *Angew. Chem., Int. Ed.*, 2010, **49**, 6400.
8 N. Zhang, S. X. Ouyang, P. Li, Y. J. Zhang, G. C. Xi, T. Kako and J. H. Ye, *Chem. Commun.*, 2011, **47**, 2041.
9 M. Halmann, M. Ulman and B. A. Blajeni, *Sol. Energy*, 1983, **31**, 429; B. A. Blajeni, M. Halmann and J. Manassen, *Sol. Energy*, 1980, **25**, 165; H. Zhou, J. Guo, P. Li, T. Fan, D. Zhang and J. Ye, *Sci. Rep.*, 2013, **3**, 1667, DOI: 10.1038/srep.01667.
10 V. Jeyalakshmi, R. Mahalakshmy, K. R. Krishnamurthy and B. Viswanathan, *6th Asia Pacific Congress on Catalysis-APCAT-6*, Taipei, Tai, Oct 13–17, 2013.
11 K. Iizuka, T. Wato, Y. Miseki, K. Saito and A. Kudo, *J. Am. Chem. Soc.*, 2011, **133**, 20863.
12 A. Kudo and Y. Miseki, *Chem. Soc. Rev.*, 2009, **38**, 253.
13 H. Jeong, T. Kim, D. Kim and K. Kim, *Int. J. Hydrogen Energy*, 2006, **31**, 1142.
14 M. Yoshino, M. Kakihana, W. S. Cho, H. Kato and A. Kudo, *Chem. Mater.*, 2002, **14**, 3369.
15 K. Rajalakshmi, V. Jeyalakshmi, K. R. Krishnamurthy and B. Viswanathan, *Indian J. Chem., Sect. A: Inorg., Bio-inorg., Phys., Theor. Anal. Chem.*, 2012, **51**, 411.
16 U. Sulaeman, S. Yin and T. Sato, *J. Nanomaterials*, 2010, **2010**, 629727.
17 J. Wang, H. Li, H. Li, S. Yin and T. Sato, *Solid State Sci.*, 2009, **11**, 182.
18 X. Zhou, J. Shi and C. Li, *J. Phys. Chem. C*, 2011, **115**, 8305.
19 T. Ohno, T. Tsubota, Y. Nakamura and K. Sayama, *Appl. Catal., A*, 2005, **288**, 74.
20 D. C. Meyer, A. A. Levin, T. Leisegang, E. Gutmann, P. Paufler, M. Reibold and W. Pompe, *Appl. Phys. A: Mater. Sci. Process.*, 2006, **84**, 31.
21 T.-H. Xie, X. Sun and J. Lin, *J. Phys. Chem. C*, 2008, **112**, 9753.
22 F. J. Morin and J. R. Oliver, *Phys. Rev. B: Solid State*, 1973, **8**, 5847.

23 J. Wang, Y. Shu and T. Sato, *J. Photochem. Photobiol., A*, 2007, **187**, 72.
24 C. S. Gopinath, *J. Phys. Chem. B*, 2006, **110**, 7079.
25 M. Satish, B. Viswanathan, R. P. Viswanath and C. S. Gopinath, *Chem. Mater.*, 2005, **17**, 6349.
26 M. Anpo and M. Takeuchi, *J. Catal.*, 2003, **216**, 505.
27 C. D. Valentin, G. Pacchioni, A. Selloni, S. Livraghi and E. Giamello, *J. Phys. Chem. B*, 2005, **109**, 11414.
28 D. Valentin, E. Finazzi, G. Pacchioni, A. Selloni, S. Livraghi, M. C. Paganini and E. Giamello, *Chem. Phys.*, 2007, **339**, 44.
29 J. Carlos and N. Perez, *Synthesis, electrical conductivity and non-stoichiometry of doped layered perovskites*, Ph.D thesis, Massachsetts Institute of Technology, USA, 1999.
30 Y. Yang and C. Tian, *Res. Chem. Intermed.*, 2010, **36**, 889.
31 M. R. Hoffman, S. T. Martin, W. Choi and D. W. Bahnemann, *Chem. Rev.*, 1995, **95**, 69; S. T. Martin, H. Herrmann, W. Choi and M. R. Hoffmann, *Trans. Faraday Soc.*, 1994, **90**, 3315; Y. H. Zhang and A. Reller, *Mater. Sci. Eng., C*, 2002, **19**, 323.
32 W. Choi, A. Termin and M. R. Hoffmann, *J. Phys. Chem.*, 1994, **98**, 13669.
33 P. Goswami and J. N. Ganguli, *Mater. Res. Bull.*, 2012, **47**, 2077.
34 Y. Cong, J. Zhang, F. Chen and M. Anpo, *J. Phys. Chem. C*, 2007, **111**, 6976.
35 Y. Liu, J. Liu, Y. Lin, Y. Zhang and Y. Wei, *Ceram. Int.*, 2009, **35**, 3061.
36 K. J. Antony Raj and B. Viswanathan, *ACS Appl. Mater. Interfaces*, 2009, **1**, 2462.
37 A. L. Linsebigler, G. Lu and J. T. Yates, *Chem. Rev.*, 1995, **95**, 735.